AIMS Materials Science, 13(2): 300–314.
DOI: 10.3934/matersci.2026017
Received: 03 February 2026
Revised: 07 March 2026
Accepted: 16 March 2026
Published: 07 April 2026

https://www.aimspress.com/journal/Materials

Research article

Effects of Cr and Er microalloying on the microstructural evolution and mechanical properties of high-pressure die-cast Al-Si-Ni alloys

Peng Hu*, Xiaolu Hong, Liying Cui, Jiang Zhang, Yinjiang Peng and Dahui Chen

Ningbo Branch of Chinese Academy of Ordnance Science, Ningbo, 315103 China

* **Correspondence:** Email: hupeng0505@163.com; Tel: (+86) 185-1041-0405.

Abstract: The effects of Cr and Er microalloying on the microstructural evolution and mechanical properties of high-pressure die-cast hypereutectic Al-Si-Ni alloys were systematically investigated. The morphology and distribution of primary Si were quantitatively analyzed using optical microscopy and ImageJ software, and the tensile properties were evaluated at room temperature and 350 °C. The results indicate that Cr addition promotes the formation of $CrSi_2$ phases, which act as heterogeneous nucleation sites, increasing the nucleation rate and suppressing the growth of primary Si. Er addition refines primary Si through interfacial segregation and the modification of growth kinetics; however, excessive Er leads to the precipitation of Al_3Er and weakens the refinement effect. As a result of the refined and more homogeneous distribution of primary Si, both Cr- and Er-containing alloys exhibited enhanced tensile strength and ductility at room temperature and 350 °C. The 0.4Cr alloy showed the best mechanical performance among the investigated compositions, and the optimal Er addition was identified to be approximately 0.2 wt.%. This work provides guidance for the microalloying design of hypereutectic Al-Si-Ni alloys with improved high-temperature mechanical performance.

Keywords: hypereutectic Al-Si-Ni alloy; microalloying; primary Si; mechanical properties

1. Introduction

Driven by the increasing demand for lightweight design, aluminum alloys have attracted considerable attention in the automotive industry, particularly for powertrain applications [1,2]. Among them, Al-Si alloys are widely used in engine components, such as pistons and cylinder heads,

owing to their high strength-to-weight ratio, excellent castability, low thermal expansion coefficient, and good wear resistance [3–5]. With the continuous pursuit of higher engine efficiency, advanced technologies, such as turbocharging and direct fuel injection, have been adopted, resulting in increased combustion temperatures and pressures, which can reach approximately 300 °C and 200 bar, respectively [6]. Consequently, conventional Al-Si alloys face challenges in maintaining sufficient mechanical strength and microstructural stability at elevated temperatures, highlighting the urgent need for further enhancement of their high-temperature performance.

Microalloying has been widely demonstrated as one of the most effective strategies for improving the high-temperature performance of Al-Si alloys. In Al-Si systems, the effects of microalloying elements can generally be classified into two primary categories. The first involves the formation of thermally stable strengthening phases that can effectively sustain mechanical strength at elevated temperatures. Representative examples include Cu and Ni additions, which are among the most extensively studied elements for high-temperature strengthening. The addition of a small amount of Cu (~0.5 wt.%) to Al-Si-Mg alloys promotes the formation of thermally resistant Q-$Al_5Mg_8Cu_2Si_6$ precipitates, resulting in enhanced strength in the temperature range of 150–250 °C [7–9]. At higher Cu levels, our previous studies have demonstrated that ~3.5 wt.% Cu addition in Al-9Si alloys leads to significant strength improvement at both 250 and 300 °C due to the formation of θ′ precipitates [4]. Similarly, Ni addition has been widely reported to enhance the high-temperature performance of Al-Si alloys by forming thermally stable Ni-bearing intermetallic phases, such as Al_3Ni and δ-Al_3CuNi, which effectively retard softening at elevated temperatures [10–12]. Beyond Cu and Ni, other transition elements, including Mo and Mn, have also been shown to promote the formation of fine, coarsening-resistant dispersoids, thereby contributing to improved yield strength at temperatures approaching 300 °C [13–16].

The second important role of microalloying lies in modifying the morphology and distribution of primary and eutectic Si phases, which is critical for reducing local stress concentration and improving mechanical performance. Traditional modifiers, such as Sr and Sb, are well known to transform the morphology of eutectic Si from coarse acicular plates into fine fibrous structures, thereby improving ductility and strength [17,18]. In recent years, rare earth elements have attracted increasing attention due to their strong interfacial activity. For example, Er has been reported to effectively refine both primary and eutectic Si, resulting in simultaneous improvements in strength and ductility [19,20]. In addition, Li et al. [21] revealed that Cr addition increases the nucleation undercooling of primary Si, facilitating heterogeneous nucleation and suppressing its growth. Similarly, Ce addition has been shown to refine Si phases and significantly enhance both strength and elongation in Al-Si alloys [22].

Although considerable efforts have been devoted to understanding the effects of microalloying on the microstructural evolution and mechanical properties of hypereutectic Al-Si alloys, most existing studies focus on gravity-cast or permanent-mold-cast alloys. In contrast, systematic investigations on hypereutectic Al-Si alloys fabricated by high-pressure die casting (HPDC), a process widely used in the automotive industry, remain limited.

In this work, the effects of Cr and Er microalloying on the microstructural evolution and mechanical properties of high-pressure die-cast hypereutectic Al-Si-Ni alloys were systematically investigated. The morphology and size distribution of primary Si in alloys containing different Cr and Er contents were characterized by optical microscopy (OM) and quantitatively analyzed using ImageJ software. Furthermore, the tensile properties at both room temperature (RT) and 350 °C were evaluated

to establish clear microstructure-property relationships, thereby providing guidance for the microalloying design of heat-resistant Al-Si alloys for advanced engine applications.

2. Materials and methods

Three Cr-containing Al14Si3.5Ni alloys with Cr contents of 0, 0.2, and 0.4 wt.% and four Er-containing Al15Si3.5Ni alloys with Er contents of 0, 0.1, 0.2, and 0.3 wt.% were prepared by HPDC to investigate the effects of Cr and Er microalloying on the microstructural evolution and mechanical properties of hypereutectic Al-Si-Ni alloys. Cylindrical castings with a diameter of 140 and a height of 50 mm were fabricated using a 500-ton die-casting machine under an applied pressure of 120 MPa and a holding time of 2 min. The alloys were melted in an electric resistance furnace at approximately 780 °C. After complete melting, a refining treatment was conducted, followed by a holding period of 20 min prior to casting. Subsequently, the casting was carried out at a melt temperature of approximately 760 °C. The chemical compositions of the experimental alloys were determined by inductively coupled plasma atomic emission spectroscopy (ICP-AES), and the measured compositions were summarized in Table 1. It should be noted that the Cr-containing and Er-containing alloy series were fabricated in two independent casting batches, which led to a slight difference in the measured Si content between the two series. Nevertheless, within each individual alloy series, the Si and Ni contents were strictly controlled to remain constant. Therefore, the variations in microstructural evolution and mechanical properties discussed in this work can be reliably attributed to the respective Cr or Er microalloying additions rather than to compositional fluctuations.

For microstructural characterization, as-cast samples were sectioned from the castings and prepared using standard metallographic procedures. Optical microscopy (OM, NM910TR) and a scanning electron microscopy (SEM, QUANTA FEG 250) equipped with energy-dispersive X-ray spectroscopy (EDS) were employed to examine the microstructure and identify the phase constituents. Quantitative analysis of the size and distribution of primary Si was performed using ImageJ software. At least four randomly selected fields of view were analyzed for each sample to ensure statistical reliability.

Table 1. Chemical compositions of experimental alloys (wt.%).

Designated name	Si	Ni	Mg	Zr	Ti	V	Fe	Cr	Er	Al
Al14Si3.5Ni	13.86	3.48	0.69	0.268	0.146	0.022	0.121	–	–	Bal.
0.2Cr	13.88	3.51	0.73	0.270	0.142	0.020	0.113	0.21	–	Bal.
0.4Cr	13.81	3.49	0.72	0.275	0.144	0.021	0.124	0.44	–	Bal.
Al15Si3.5Ni	14.97	3.45	0.71	0.124	0.132	0.076	0.135	–	–	Bal.
0.1Er	14.85	3.47	0.68	0.118	0.120	0.083	0.131	–	0.124	Bal.
0.2Er	14.93	3.46	0.73	0.120	0.131	0.079	0.126	–	0.215	Bal.
0.3Er	14.94	3.49	0.74	0.121	0.125	0.081	0.128	–	0.331	Bal.

Tensile tests were conducted at RT and 350 °C using an MTS E45.105 universal testing machine, in accordance with GB/T 228.1-2021 and GB/T 228.2-2015 standards. The geometry of the tensile

specimens is shown in Figure 1. At least two specimens were tested under each condition, and the reported mechanical properties represent average values.

To ensure consistency and reliable comparisons, all samples used for microstructural characterization and mechanical testing were extracted from the same location within each casting.

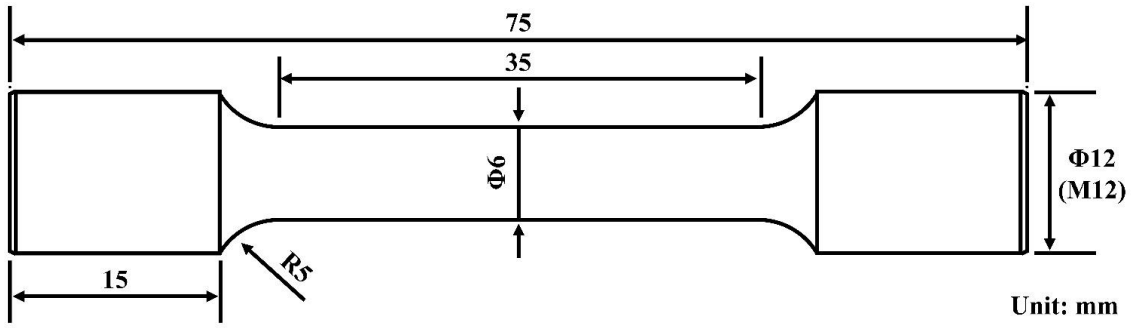

Figure 1. Schematic diagram of tensile specimens.

3. Results and discussions

3.1. Impact of Cr on the microstructural evolution and mechanical properties

Figure 2 shows a representative SEM image of the different Cr-containing Al14Si3.5Ni alloys. Microstructural analysis reveals that the addition of Cr has a negligible influence on the primary phase constituents of the hypereutectic Al-Si-Ni alloys fabricated by HPDC. The as-cast microstructure mainly consists of α-Al, eutectic Si, primary Si, Al_3Ni, and Al_3(Ni, Zr) phases. The eutectic Si predominantly exhibits a Chinese-script morphology, whereas the primary Si appears as blocky particles; both phases exhibit a black contrast in the SEM images. The gray Chinese-script phase and the needle-like phase are identified as Al_3Ni and Al_3(Ni, Zr), respectively, as confirmed by EDS analysis and previous studies [23,24].

Figure 3 presents low-magnification optical micrographs of Al14Si3.5Ni alloys containing different Cr contents. Although the overall phase constituents remain largely unchanged, pronounced variations in the morphology, size, and distribution of primary Si are observed with increasing Cr addition. In particular, the number density, characteristic length, and volume fraction of primary Si show systematic changes, as summarized in Figures 4 and 5. Moreover, Cr addition leads to a noticeable modification in the morphology of primary Si, which evolves from irregular blocky shapes to more regular tetragonal or hexagonal morphologies.

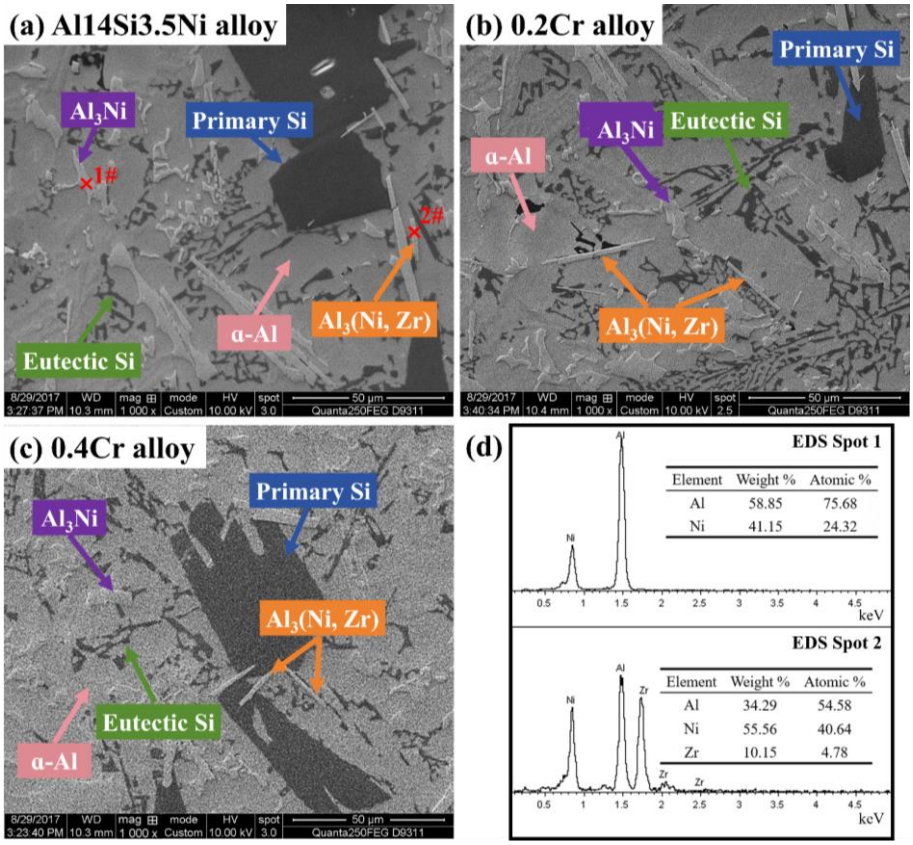

Figure 2. Typical SEM images of varying Cr-containing Al-Si-Ni alloy: (a) Al14Si3.5Ni alloy, (b) 0.2Cr alloy, (c) 0.4Cr alloy, and (d) the corresponding EDS results.

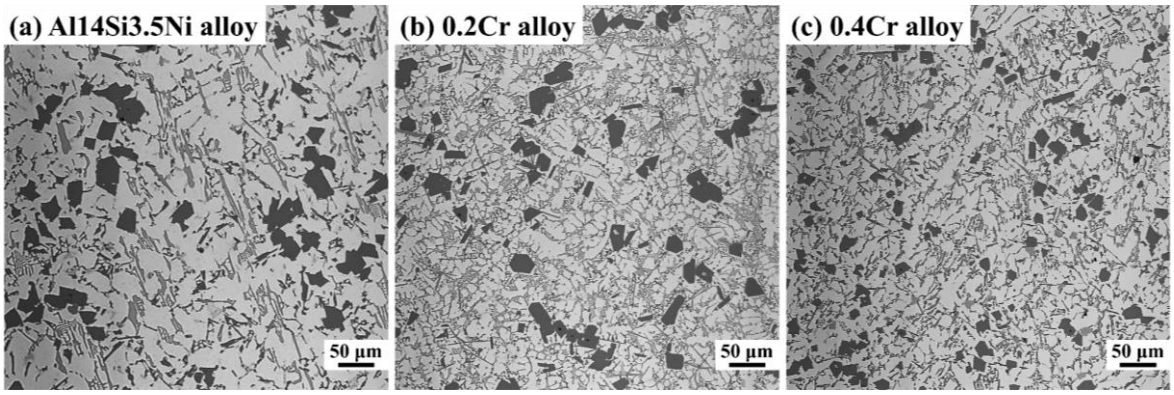

Figure 3. Low-magnification OM images of varying Cr-containing Al-Si-Ni alloy: (a) Al14Si3.5Ni alloy, (b) 0.2Cr alloy, and (c) 0.4Cr alloy.

Figure 4 illustrates the quantified number density and volume fraction of primary Si in Al14Si3.5Ni alloys with varying Cr contents. As the Cr concentration increased from 0 to 0.4 wt.%, the number density of primary Si increased markedly from 1.5×10^{-4} to 3.2×10^{-4} μm^{-2}, corresponding to an increment of approximately 113%. In contrast, the volume fraction of primary Si decreased significantly from 10.6% to 6.2%, representing a reduction of 41.5%. This inverse relationship between

number density and volume fraction indicates that Cr addition effectively refines primary Si by promoting the formation of a larger number of smaller particles rather than a limited number of coarse ones.

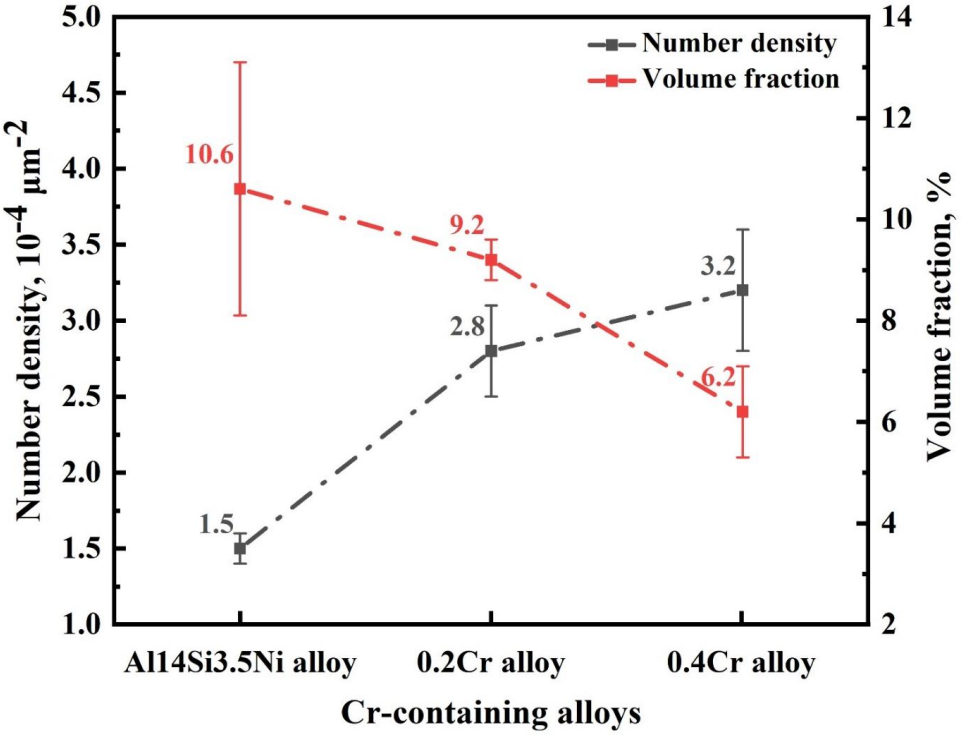

Figure 4. Summarized quantification characteristics of primary Si in different Cr-containing Al14Si3.5Ni alloys.

The size distribution of primary Si was further evaluated by measuring its characteristic lengths, as shown in Figure 5. The average length of primary Si decreased substantially from 37.7 μm in the Cr-free Al14Si3.5Ni alloy to 28.4 μm in the 0.2Cr alloy and further to 23.2 μm in the 0.4Cr alloy. Additionally, the maximum length of primary Si was reduced from approximately 100 μm in the Cr-free alloy to around 70 μm in the 0.4Cr alloy. These results confirm that Cr addition significantly suppresses the growth of primary Si and leads to a more refined and homogeneous microstructure.

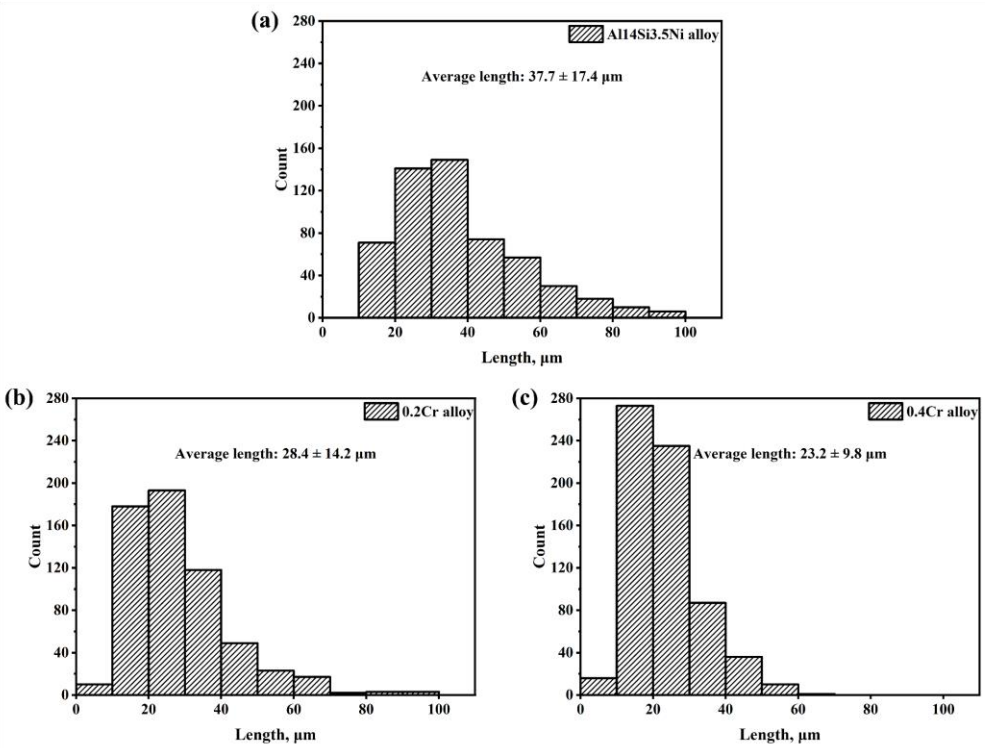

Figure 5. Quantified primary Si length distribution of varying Cr-containing Al-Si-Ni alloy: (a) Al14Si3.5Ni alloy, (b) 0.2Cr alloy, and (c) 0.4Cr alloy.

Based on the quantitative results, the introduction of Cr promotes the formation of finer primary Si, characterized by an increased number density, reduced volume fraction, and decreased particle size. This refinement effect can be primarily attributed to the role of Cr in heterogeneous nucleation. Cr atoms have a strong affinity for Si and can react with Si to form hexagonal $CrSi_2$ phases during solidification. These $CrSi_2$ particles precipitate prior to the formation of primary Si and serve as effective heterogeneous nucleation sites, thereby increasing the nucleation rate of primary Si and reducing its growth propensity [21,25]. Consequently, the combined effects of enhanced nucleation and restricted growth lead to a refined primary Si microstructure in Cr-containing Al-Si-Ni alloys.

Tensile tests were conducted on Al14Si3.5Ni alloys with different Cr contents at both RT and 350 °C, and the corresponding ultimate tensile strength (UTS) and elongation are summarized in Figure 6. At RT, both UTS and elongation increased markedly with increasing Cr content, indicating a pronounced strengthening and ductility enhancement effect induced by Cr addition. Specifically, the UTS increased from 192 MPa for the Cr-free alloy to 237 MPa for the 0.4Cr alloy, and the elongation improved from 0.5% to 0.7%.

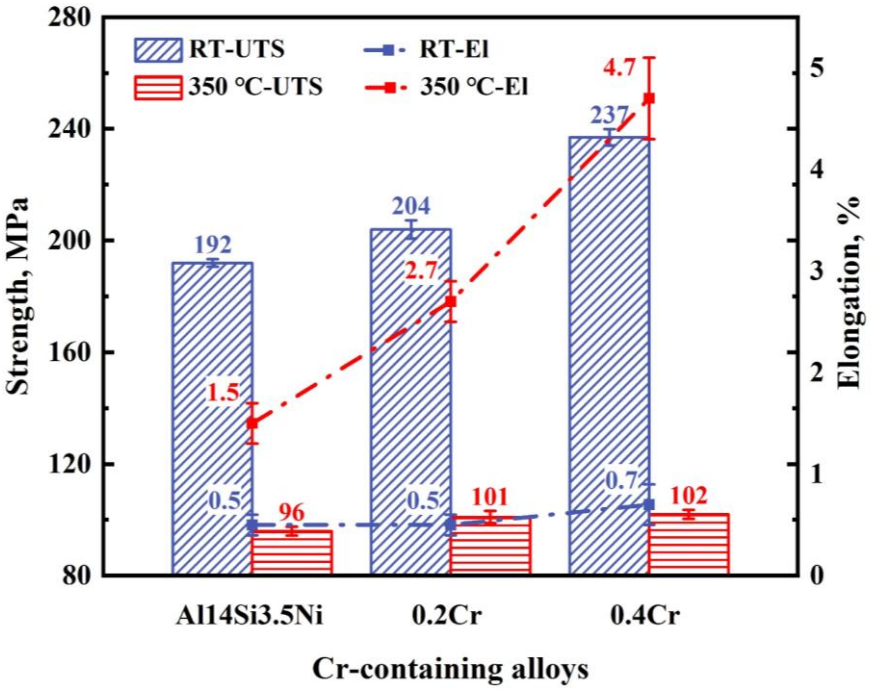

Figure 6. UTS and elongation at RT and 350 ℃ of different Cr-containing Al14Si3.5Ni alloys.

When the testing temperature was elevated to 350 °C, all alloys exhibited a substantial reduction in UTS due to thermal softening. The maximum decrease in UTS, approximately 57%, was observed in the 0.4Cr alloy. In contrast, the elongation showed a pronounced increase at elevated temperatures, rising from less than 1% at RT to a maximum value of 4.7% at 350 °C, reflecting the enhanced plastic deformation capability at high temperature. Despite the overall softening behavior at 350 °C, the alloy containing 0.4 wt.% Cr still exhibited the highest UTS (102 MPa) and elongation (4.7%) among all tested compositions, demonstrating the beneficial role of Cr addition in improving the high-temperature mechanical performance of Al-Si-Ni alloys.

The observed enhancement in tensile properties is closely correlated with the microstructural refinement induced by Cr addition. As discussed in the preceding section, Cr promotes the formation of finer and more uniformly distributed primary Si. In addition, the eutectic Si is significantly refined after Cr addition, with its morphology modified from coarse platelet-like structures to a finer fibrous form (Figure 3). The refinement and uniform distribution of eutectic Si enhance the load-transfer capability and reduce stress localization, thereby contributing substantially to strength improvement. Meanwhile, the reduction in size and irregularity of primary Si particles alleviates stress concentration at sharp edges and delays crack initiation during tensile deformation. As a result, both strength and ductility are synergistically improved in the Cr-containing Al-Si-Ni alloys at both RT and elevated temperature.

3.2. Impact of Er on the microstructural evolution and mechanical properties

Figure 7 presents representative low-magnification optical micrographs of Al15Si3.5Ni alloy containing different Er additions. The typical phase constituents in the Al15Si3.5Ni alloy are identical to those in the Al14Si3.5Ni alloy. In addition, similar to the effect observed for Cr, Er addition induces

pronounced variations in the morphology, size, and length distribution of primary Si. Systematic changes in the number density, characteristic length, and volume fraction of primary Si are quantitatively summarized in Figures 8 and 9.

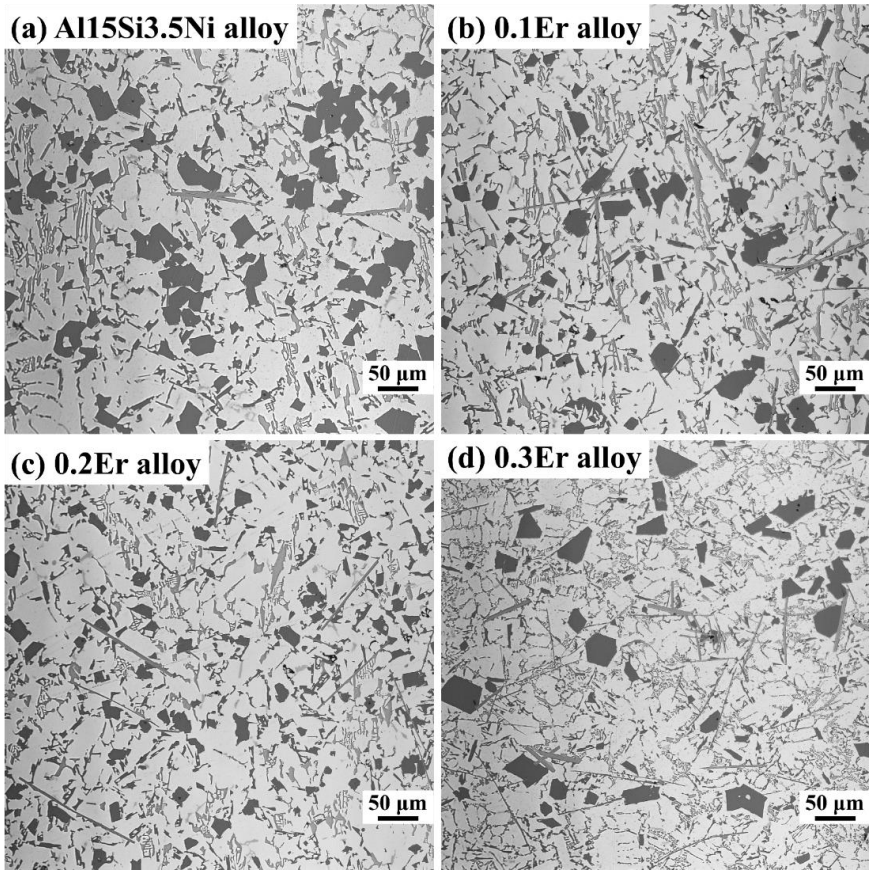

Figure 7. Low–magnification OM images of varying Er-containing Al-Si-Ni alloy: (a) Al15Si3.5Ni alloy, (b) 0.1Er alloy, (c) 0.2Er alloy, and (d) 0.3Er alloy.

Figure 8 shows the quantified number density and volume fraction of primary Si as a function of Er content (0–0.3 wt.%). With increasing Er concentration, the number density of primary Si initially increased from 1.7×10^{-4} μm^{-2} in the Er-free Al15Si3.5Ni alloy to a maximum of 2.4×10^{-4} μm^{-2} in the 0.2Er alloy, followed by a decrease to 2.0×10^{-4} μm^{-2} in the 0.3Er alloy. In contrast, the volume fraction of primary Si decreased from 11.7% in the Er-free alloy to 5.7% in the 0.2Er alloy, and then slightly increased to 5.9% in the 0.3Er alloy. Accordingly, the 0.2Er alloy exhibits the optimal refinement effect, characterized by the highest number density and the lowest volume fraction of primary Si.

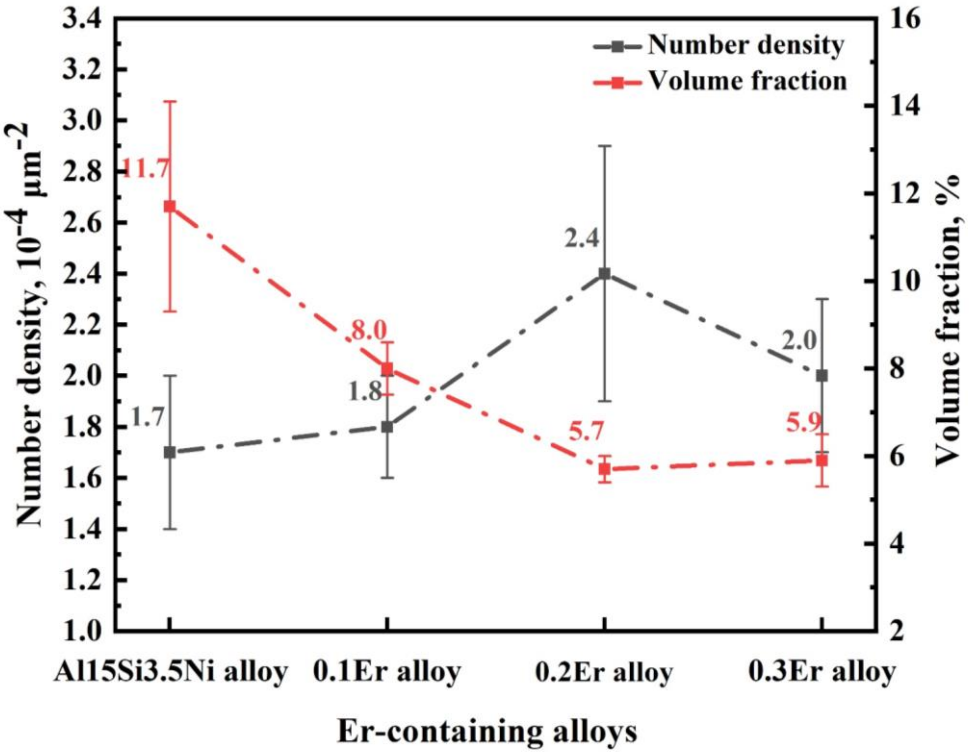

Figure 8. Summarized quantification characteristics of primary Si in different Er-containing Al15Si3.5Ni alloys.

The size distribution of primary Si in Er-containing alloys is shown in Figure 9. The average length of primary Si decreased monotonically from 38.3 μm in the Er-free alloy to 29.2, 24.4, and 20.6 μm in the alloys containing 0.1, 0.2, and 0.3 wt.% Er, respectively. Meanwhile, the maximum length of primary Si was significantly reduced from approximately 140 μm in the Er-free alloy to about 90 μm in the 0.3Er alloy. Notably, despite its smaller average length, the 0.3Er alloy exhibited a more heterogeneous size distribution compared with the 0.2Er alloy, as evidenced by Figures 7 and 9. This non-uniformity resulted in a reduced number density and a slightly increased volume fraction of primary Si in the 0.3Er alloy relative to the 0.2Er alloy.

Overall, these results confirm that Er addition also promotes the refinement and homogenization of primary Si in hypereutectic Al-Si-Ni alloys produced by HPDC, although the refining efficiency exhibits a non-monotonic dependence on Er content. The refinement mechanism can be attributed to the limited solubility of Er in both Al and Si. During solidification, Er atoms tend to segregate to the solid-liquid interface of growing Si phases and adsorb onto growth steps, thereby modifying the interfacial growth kinetics and suppressing the anisotropic growth of primary Si, leading to morphological refinement [20,26]. In addition, Er atoms can accumulate ahead of the advancing solid-liquid interface, further restricting Si growth.

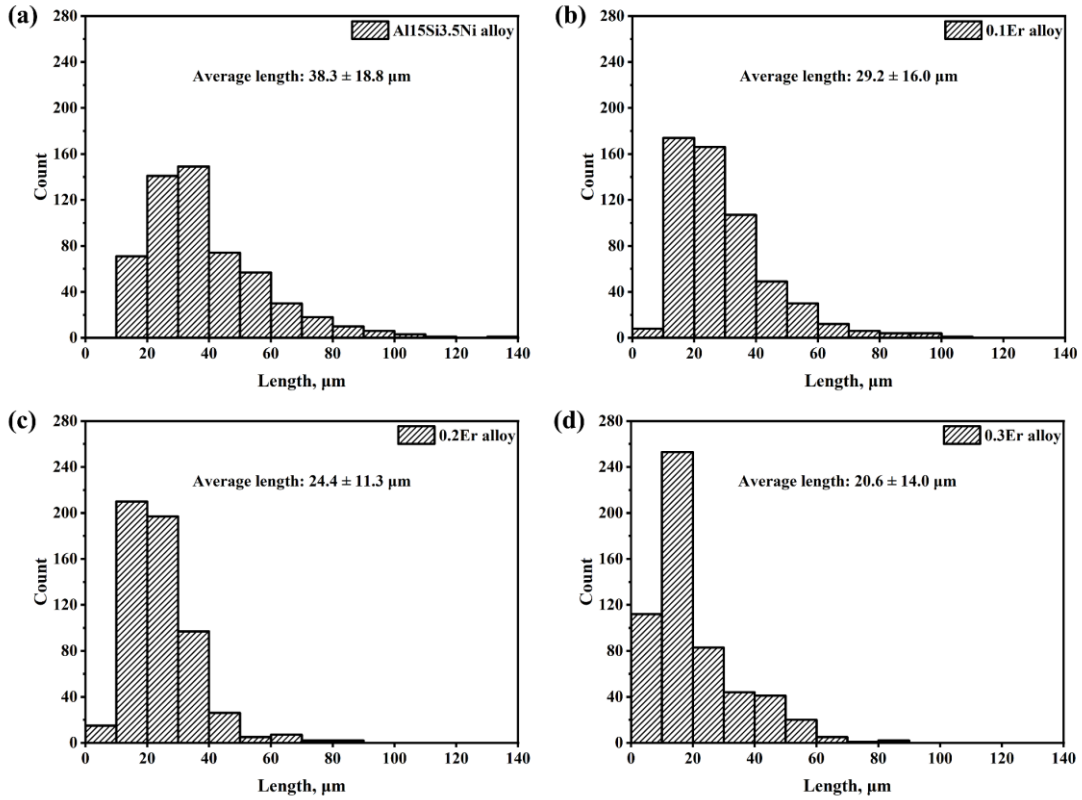

Figure 9. Quantified primary Si length distribution of varying Er-containing Al-Si-Ni alloy: (a) Al15Si3.5Ni alloy, (b) 0.1Er alloy, (c) 0.2Er alloy, and (d) 0.3Er alloy.

However, when the Er content exceeds an optimal level (e.g., 0.3 wt.% in the present study), the local Er concentration can approach the eutectic composition, promoting the precipitation of Al_3Er phases [20,27]. The formation of Al_3Er consumes free Er atoms in the melt, thereby weakening the interfacial modification effect of Er on primary Si. As a result, the refinement efficiency deteriorates, leading to partial coarsening and a less uniform distribution of primary Si in the 0.3Er alloy.

The UTS and elongation of Al15Si3.5Ni alloys with varying Er contents tested at both RT and 350 °C are presented in Figure 10. At both testing temperatures, UTS and elongation exhibited a non-monotonic dependence on Er content. Specifically, at RT, the UTS and elongation increased from 220 MPa and 1.3% in the Er-free alloy to peak values of 229 MPa and 1.5% in the 0.2Er alloy, followed by a decrease to 212 MPa and 1.0% in the 0.3Er alloy. A similar trend was also observed at 350 °C, where the UTS and elongation increased from 93 MPa and 4.8% in the Er-free alloy to 103 MPa and 6.3% in the 0.2Er alloy and then decreased slightly to 94 MPa and 6.0% in the 0.3Er alloy.

Despite the pronounced thermal softening experienced by all Er-containing alloys at 350 °C, the alloy with 0.2 wt.% Er consistently exhibited the highest UTS and elongation at both RT and elevated temperature. This behavior highlights the existence of an optimal Er addition for enhancing the mechanical performance of Al-Si-Ni alloys.

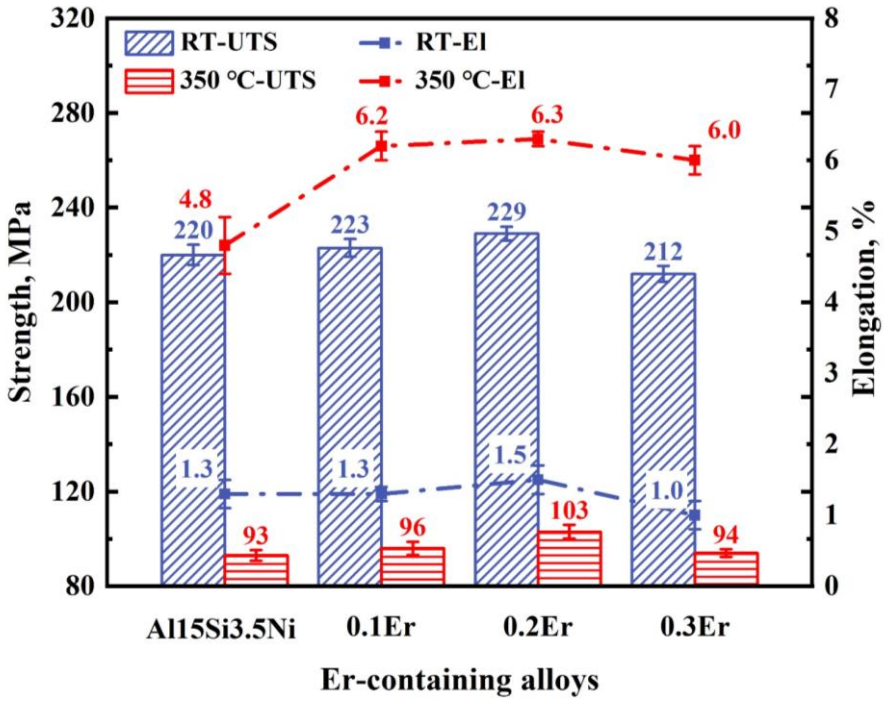

Figure 10. UTS and elongation at RT and 350 °C of different Er-containing Al15Si3.5Ni alloys.

Similar to the effect of Cr addition, the improvement in tensile properties induced by Er can be also correlated with microstructural refinement. For the 0.2Er alloy, the formation of finer and more uniformly distributed primary Si effectively reduces local stress concentrations and delays crack initiation during tensile deformation, leading to a simultaneous improvement in both strength and ductility. In contrast, when the Er content increases to 0.3 wt.%, the precipitation of Al_3Er consumes a substantial portion of Er from the melt, thereby weakening its refinement capability. As a result, primary Si exhibits partial coarsening and a less homogeneous distribution, which in turn causes a slight deterioration in mechanical properties at both room temperature and 350 °C.

4. Conclusions

The effects of Cr and Er microalloying on the distribution of primary Si and the mechanical properties of hypereutectic Al-Si-Ni alloys fabricated by HPDC were systematically investigated. The main conclusions can be summarized as follows:

(1) The incorporation of Cr promotes the formation of $CrSi_2$ phases, which act as effective heterogeneous nucleation sites for primary Si. This increases the nucleation rate and suppresses the growth of primary Si, leading to a refined morphology of primary Si in hypereutectic Al-Si-Ni alloys.

(2) Er addition leads to interfacial segregation at the solid-liquid interface of growing Si phases, where Er atoms adsorb onto growth steps and modify interfacial growth kinetics, thereby suppressing the anisotropic growth of primary Si. However, excessive Er promotes the precipitation of Al_3Er, which consumes available Er in the melt and weakens its refinement effect.

(3) The refinement and homogenization of primary Si induced by Cr and Er microalloying effectively reduce local stress concentrations and delay crack initiation, resulting in enhanced

mechanical properties of hypereutectic Al-Si-Ni alloys prepared by HPDC at both RT and 350 °C. Under the present experimental conditions, the 0.4Cr alloy exhibits the best mechanical performance among the compositions investigated, and the optimal Er content is approximately 0.2 wt.%.

(4) This study clarifies the distinct mechanisms by which Cr and Er microalloying regulate the nucleation and growth of primary Si, providing useful guidance for the microstructural design and performance optimization of hypereutectic Al-Si alloys for high-temperature structural applications.

Acknowledgments

This work was supported by Natural Science Foundation of Inner Mongolia Autonomous Region of China (grants No. 2025QN05019 and No. 2025QN05063), Zhejiang Provincial Postdoctoral Science Foundation (grants No. ZJ2025160 and No. ZJ2025161), and China Postdoctoral Science Foundation (grant No. 2025M784431).

Conflict of interest

The authors declare no conflict of interest.

Use of AI tools declaration

The authors declare they have not used Artificial Intelligence (AI) tools in the creation of this article.

Author contributions

Peng Hu: conceptualization, methodology, investigation, formal analysis and writing-original draft; Xiaolu Hong: validation, review and editing; Liying Cui: investigation, methodology, review and editing; Jiang Zhang: investigation, data curation and editing; Yinjiang Peng: review and editing; Dahui Chen: conceptualization, methodology, review and editing.

References

1. Alan T, Emmanuel DM, Alan L, et al. (2019) Materials for automotive lightweighting. *Annu Rev Mater Res* 49: 327–359. https://doi.org/10.1146/annurev-matsci-070218-010134
2. Cui L, Zhang Z, Chen XG (2024) Lightweight Al-based entropy alloys: Overview and future trend. *Sci China Mater* 67: 31–46. https://doi.org/10.1007/s40843-023-2699-2
3. Ye H (2003) An overview of the development of Al-Si-alloy based material for engine applications. *J Mater Eng Perform* 12: 288–297. https://doi.org/10.1361/105994903770343132
4. Hu P, Pan L, Chen XG (2024) Elevated-temperature performances of Al-Si-Cu casting alloys for cylinder head applications. *Mate Charact* 218: 114484. https://doi.org/10.1016/j.matchar.2024.114484
5. Hu P, Liu K, Pan L, et al. (2024) Thermomechanical fatigue behavior and its life prediction of AlSi9Cu3.5 cast alloy. *J Mater Sci* 59: 8022–8039. https://doi.org/10.1007/s10853-024-09663-9

6. European Aluminium Association (2015) The aluminium automotive manual: Joining dissimilar materials, 1–31. Available from: https://european-aluminium.eu/blog/aluminium-automotive-manual/.
7. Farkoosh AR, Pekguleryuz M (2015) Enhanced mechanical properties of an Al-Si-Cu-Mg alloy at 300 °C: Effects of Mg and the Q-precipitate phase. *Mater Sci En A* 621: 277–286. https://doi.org/10.1016/j.msea.2014.10.080
8. Mørtsell EA, Qian F, Marioara CD, et al. (2019) Precipitation in an A356 foundry alloy with Cu additions-A transmission electron microscopy study. *J Alloys Compd* 785: 1106–1114. https://doi.org/10.1016/j.jallcom.2019.01.229
9. Srinivas D, Gowrishankar MC, Hiremath P, et al. (2022) Influence of various trace metallic additions and reinforcements on A319 and A356 alloys-A review. *Cogent Eng* 9: 2007746. https://doi.org/10.1080/23311916.2021.2007746
10. Belov NA, Eskin DG, Avxentieva NN (2005) Constituent phase diagrams of the Al-Cu-Fe-Mg-Ni-Si system and their application to the analysis of aluminium piston alloys. *Acta Mater* 53: 4709–4722. https://doi.org/10.1016/j.actamat.2005.07.003
11. Asghar Z, Requena G, Boller E (2011) Three-dimensional rigid multiphase networks providing high-temperature strength to cast AlSi10Cu5Ni1-2 piston alloys. *Acta Mater* 59: 6420–6432. https://doi.org/10.1016/j.actamat.2011.07.006
12. Farkoosh AR, Javidani M, Hoseini M, et al. (2013) Phase formation in as-solidified and heat-treated Al-Si-Cu-Mg-Ni alloys: Thermodynamic assessment and experimental investigation for alloy design. *J Alloys Compd* 551: 596–606. https://doi.org/10.1016/j.jallcom.2012.10.182
13. Liu K, Wang S, Hu P, et al. (2023) Improved thermos-mechanical fatigue resistance of Al-Si-Cu 319 alloys by microalloying with Mo. *Materials* 16: 3515. https://doi.org/10.3390/ma16093515
14. Jin L, Liu K, Chen XG (2020) Evolution of dispersoids and their effects on elevated-temperature strength and creep resistance in Al-Si-Cu 319 cast alloys with Mn and Mo additions. *Mater Sci Eng A* 770: 138554. https://doi.org/10.1016/j.msea.2019.138554
15. Farkoosh AR, Chen XG, Pekguleryuz M (2015) Dispersoid strengthening of a high-temperature Al-Si-Cu-Mg alloy via Mo addition. *Mater Sci Eng A* 620: 181–189. https://doi.org/10.1016/j.msea.2014.10.004
16. Liu K, Chen XG (2018) Improvement in elevated-temperature properties of Al-13%Si piston alloys by dispersoid strengthening via Mn addition. *J Mater Res* 33: 3430–3438. https://doi.org/10.1557/jmr.2018.117
17. Wang QG, Apelian D, Lados DA (2001) Fatigue behavior of A356/357 aluminum cast alloys. Part II-Effect of microstructural constituents. *J Light Met* 1: 85–97. https://doi.org/10.1016/S1471-5317(00)00009-2
18. Fatahalla N, Hafiz M, Abdulkhalek M (1999) Effect of microstructure on the mechanical properties and fracture of commercial hypoeutectic Al-Si alloy modified with Na, Sb and Sr. *J Mater Sci* 34: 3555–3564. https://doi.org/10.1023/A:1004626425326
19. Xing P, Gao B, Zhuang Y, et al. (2010) On the modification of hypereutectic Al-Si alloys using rare earth Er. *Acta Metal Sin (Engl Lett)* 23: 327–333. https://doi.org/10.11890/1006-7191-105-327
20. Li Q, Xia T, Lan Y, et al. (2013) Effects of rare earth Er addition on microstructure and mechanical properties of hypereutectic Al-20%Si alloy. *Mater Sci Eng A* 588: 97–102. https://doi.org/10.1016/j.msea.2013.09.017

21. Li C, Liu F, Yu F, et al. (2023) The growth mechanism and morphology evolution of primary Si during slow cooling solidification of high-purity Al-15Si alloy with Cr additions. *J Mater Re Technol* 23: 1204–1213. https://doi.org/10.1016/j.jmrt.2023.01.034
22. Li Q, Xia T, Lan Y, et al. (2013) Effect of rare earth cerium addition on the microstructure and tensile properties of hypereutectic Al-20%Si alloy. *J Alloys Compd* 562: 25–32. https://doi.org/10.1016/j.jallcom.2013.02.016
23. Böyük U, Engin S, Maraşlı N (2011) Microstructural characterization of unidirectional solidified eutectic Al-Si-Ni alloy. *Mater Charact* 62: 844–851. https://doi.org/10.1016/j.matchar.2011.05.010
24. Lee YH, Kayani SH, Lee JM, et al. (2025) Role of Ni in high elastic modulus Al-Si-Ni alloys: Solidification and microstructure evolution. *Mater Charact* 115768. https://doi.org/10.1016/j.matchar.2025.115768
25. Galkin NG, Velitchko TV, Skripka SV, et al. (1996) Semiconducting and structural properties of $CrSi_2$ A-type epitaxial films on Si (111). *Thin Solid Films* 280: 211–220. https://doi.org/10.1016/0040-6090(95)08241-7
26. Lu SZ, Hellawell A (1987) The mechanism of silicon modification in aluminum-silicon alloys: Impurity-induced twinning. *Metall Trans A* 18: 1721–1733. https://doi.org/10.1007/BF02646204
27. Yang D, Li X, He D, et al. (2013) Effect of minor Er and Zr on microstructure and mechanical properties of Al−Mg−Mn alloy (5083) welded joints. *Mater Sci Eng A* 561: 226–231. https://doi.org/10.1016/j.msea.2012.11.002